# EFFECT OF TRANSVERSE PRESTRESSING ON SHEAR BEHAVIORS OF HIGH-STRENGTH CONCRETE COLUMNS

**Y. Shinohara**[1]

[1] *Assoc. Professor, Structural Engineering Research Center, Tokyo Institute of Technology, Yokohama, Japan*
*Email: shinohara.y.ab@m.titech.ac.jp*

**ABSTRACT :**
Experiments and 3-D FEM analyses were performed on high-strength concrete columns laterally prestressed by high-strength shear reinforcement in order to study the influence of active confinement on the shear strength and crack behaviors. Lateral prestress was introduced in proportion to the concrete strength, and the width of every crack near the transverse reinforcement was measured by a digital microscope. By increasing the lateral prestress as mentioned above, the shear crack strength and ultimate shear strength increased, but the effectiveness of active confinement was weakened as the axial force ratio decreased. FEM analyses can be used to evaluate the shear crack strength and the ultimate shear strength, and to explain the effect of active confinement on shear behaviors because FEM analyses evaluates the intensity of confinement in a tri-axial state of stress with minor principal stress as well as the degree of damage for compressive failures.

**KEYWORDS:** High-strength concrete, Lateral prestress, Active confinement, Shear behavior

## 1. INTRODUCTION

Prestressing concrete structures is generally performed to control flexural cracks because prestressing arranges the tendons in the axial direction of a given member. On the other hand, in an attempt to delay the onset of shear cracking and to reduce the crack width, experimental studies have been conducted on reinforced concrete (RC) columns, which have been laterally prestressed by high-strength shear reinforcement [Watanabe et al. 2004]. The results of these flexure-shear tests have indicated that transverse prestressing increases the shear capacity at the first diagonal cracking (shear crack strength) and remarkably decreases the width of shear cracks, especially their residual openings. This reduction of the crack opening improves earthquake resistance and durability.
The main objectives of the present study are (1) to investigate how transverse prestressing in high-strength concrete columns affects the shear behavior with respect to the propagation of cracks and the triaxial state of stress, and (2) to quantitatively estimate the effect of active confinement on shear behaviors based on the triaxial state of stress in the concrete by 3D FEM analyses.

## 2. OVERVIEW OF TEST AND ANALYSIS

### *2.1 Test Specimens and Analytical Models*

Figure 1 shows the details of the test specimen and the finite element model. Table 1 summarizes the specifications of the specimens. The compressive strength of the concrete used in the present study was aimed to be 45 and 90 N/mm$^2$ (Fc45 and Fc90). The ratio of the axial load to axial strength for Fc90 was limited to 0.15 due to the capacity of equipment, while that for Fc45 was set to 0.15 and 0.3 in order to investigate the effect of axial load on shear crack behaviors. Flexure-shear tests were performed on RC columns that were laterally prestressed (LPRC) and not prestressed (RC). Test designation was expressed by LPRC or RC, compressive strength, and the ratio of axial load to axial strength. The test specimens had a square cross section of 340 mm x 340 mm and a height of 900 mm. The specimens were designed to reach shear failure before the longitudinal reinforcement yield, in accordance with the design guidelines of the Architectural Institute of Japan (1999). For this reason, high-strength steel bars (D22, in Fig. 1, $\sigma_y$=1187 N/mm$^2$) were used for longitudinal reinforcement. Moreover, additional rebars (D13 in Fig. 1) were arranged to prevent columns from splitting due

to bond failure. The lateral prestress, $\sigma_L$, which is proportional to the strength of the concrete, $\sigma_B$, ($\sigma_L/\sigma_B \approx 0.03$) was introduced into concrete as follows: (1) high-strength transverse hoops (U6.4, U9.0 in Fig. 1) were pretensioned to approximately 30% of the yield stress using rigid steel molds and special jigs, which are shown in Fig. 1, (2) concrete was placed vertically into the molds and cured until the strength of the concrete increased sufficiently, (3) the core concrete was laterally prestressed by removing the steel molds. The product of the ratio, $p_w$, and the stress, $\sigma_{wp}$, of the pretensioned transverse reinforcement was defined as the average lateral prestress, $\sigma_L$ ($=p_w\sigma_{wp}$), to indicate the intensity of lateral prestress. Table 2 provides the mix proportion of concrete used in the test specimens. The coarse aggregate used in the mix is natural round sea gravel with a maximum aggregate size of 25 mm. The mechanical properties of the concrete and reinforcement are shown in Figs. 2 and 3 along with their idealizations in FEM analysis.

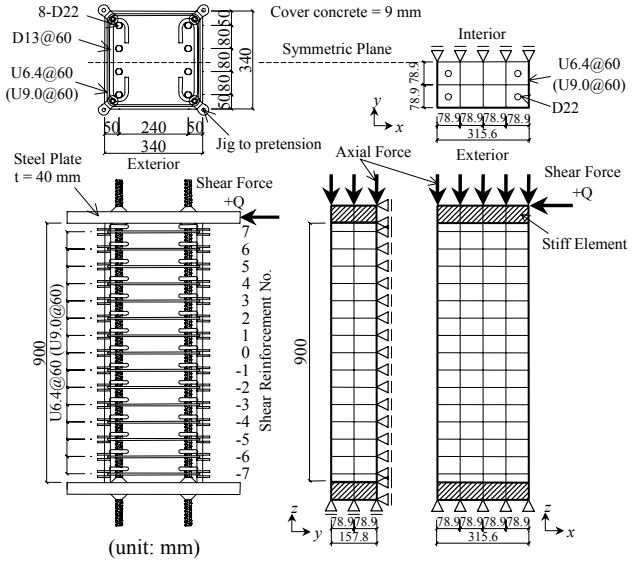


Figure 1 Details of test specimen and FE model

Table 1 List of test specimens

| Test Designation | $\sigma_B$ (N/mm$^2$) | $\sigma_0/\sigma_B$ | $p_w$ (%) | $\sigma_{wp}$ (N/mm$^2$) | $\sigma_L$ (N/mm$^2$) | $\sigma_L/\sigma_B$ |
|---|---|---|---|---|---|---|
| RC-45-0.15 | 44.2 | 0.15 | 0.29 | 0 | 0 | 0 |
| LPRC-45-0.15 | 46.2 | | | 513 | 1.5 | 0.032 |
| RC-90-0.15 | 91.9 | 0.15 | 0.63 | 0 | 0 | 0 |
| LPRC-90-0.15 | 93.0 | | | 428 | 2.7 | 0.029 |
| RC-45-0.30 | 50.8 | 0.30 | 0.29 | 0 | 0 | 0 |
| LPRC-45-0.30 | 46.5 | | | 536 | 1.6 | 0.034 |

$\sigma_B$=compressive strength of concrete, $\sigma_0$=axial stress of column, $p_w$=ratio of transverse hoop, $\sigma_{wp}$=introduced prestress in transverse hoop, $\sigma_L$=lateral prestress ($=p_w\sigma_{wp}$), RC-45-0.30 and LPRC-45-0.30 after Shinohara (2005)

Table 2 Mix proportion (Unit: kg/m$^3$)

| Nominal Strength | W / C | Water | Cement | Sand | Aggregate | Super-plasticizer |
|---|---|---|---|---|---|---|
| Fc45 | 0.50 | 184 | 373 | 762 | 945 | 0.93 |
| Fc90 | 0.30 | 155 | 517 | 857 | 861 | 3.88 |

| Test series | $\sigma_B$ N/mm$^2$ | $\varepsilon_{max}$ | $E_c$ N/mm$^2$ | $\sigma_t$ N/mm$^2$ | $W_1$ mm | $W_2$ mm | $v$ |
|---|---|---|---|---|---|---|---|
| RC-45-0.15 | 44.2 | -0.002 | 3.34E+4 | 2.6 | 0.034 | 0.17 | 0.2 |
| LPRC-45-0.15 | 46.2 | -0.002 | 3.41E+4 | 2.7 | 0.033 | 0.16 | 0.2 |
| RC-90-0.15 | 91.9 | -0.0026 | 4.21E+4 | 5.3 | 0.017 | 0.083 | 0.2 |
| LPRC-90-0.15 | 93.0 | -0.0026 | 4.30E+4 | 5.3 | 0.017 | 0.083 | 0.2 |
| RC-45-0.30 | 50.8 | -0.002 | 3.51E+4 | 2.9 | 0.031 | 0.15 | 0.2 |
| LPRC-45-0.30 | 46.5 | -0.002 | 3.45E+4 | 2.9 | 0.031 | 0.15 | 0.2 |

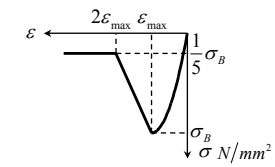


Compressive stress-strain curve

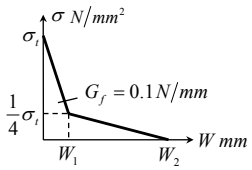


Tensile stress-crack width curve

Figure 2 Mechanical properties and analytical model for concrete

| Type | $\sigma_y$ (N/mm$^2$) | $\sigma_{max}$ (N/mm$^2$) | $E_s$ (N/mm$^2$) |
|---|---|---|---|
| D22 | 1187 | 1298 | 1.96E+5 |
| U6.4 | 1471 | 1506 | 2.05E+5 |
| U9.0 | 1405 | 1466 | 2.05E+5 |

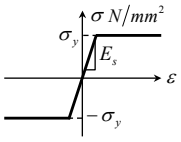


Stress-strain curve

Figure 3 Mechanical properties and analytical model for reinforcement

### *2.2 Loading and Measuring Methods in Tests*

Figure 4 shows the loading apparatus. The vertical force on the test specimen was supplied by a 2 MN hydraulic jack, and the ratio of axial load to axial strength was maintained constant at 0.15 or 0.3 during the test. The horizontal force was supplied by two hydraulic jacks with a capacity of 500 kN and 1000 kN, and the horizontal

force was controlled in displacement. The cyclic horizontal load was applied to produce an antisymmetric moment in the column. The horizontal load was reduced when the rotation angle of a column, $R$, reached ±1/400, ±1/200, ±1/100, ±1/67, and ±1/50, until it reached the peak load. Two digital microscopes, which each had a resolution of 0.01 mm, were used to measure the width of each shear crack near the shear reinforcement three times for each loading cycle and twice for each unloading cycle. The crack width used in the present study was defined as the distance normal to the direction of the crack, which is illustrated in Fig. 5. Three strain gauges, locations, and designations, which are shown in Fig. 5, were attached to each leg of the transverse hoops.

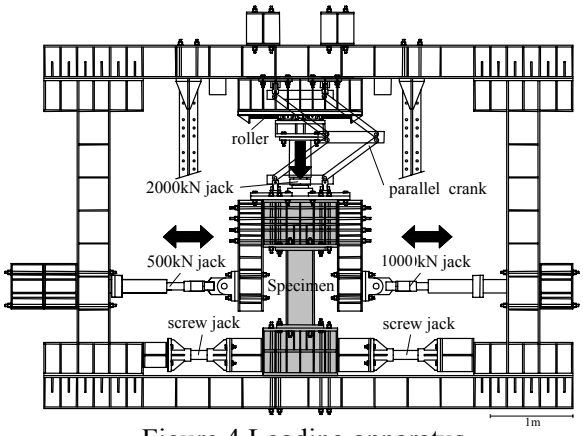


Figure 4 Loading apparatus

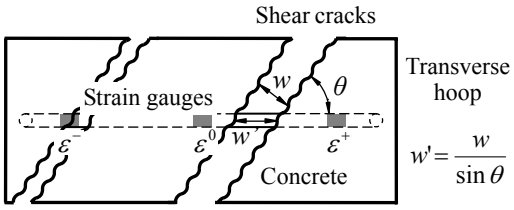


Figure 5 Definition of crack width and designation of strain gauges

### *2.3 Assumptions and Procedures in Analyses*

Figure 1 shows the finite element mesh and boundary conditions. Due to symmetry, only half of the column was analyzed. The stiff elements were attached at the top and bottom of a column to idealize the steel stubs. The top nodes were constrained to move uniformly in the vertical direction and to prevent rotation of the upper stiff elements, so that a column was deformed in an antisymmetric mode. Concrete was modeled by a twenty-node isoparametric solid brick element, and longitudinal reinforcement was embedded in the concrete elements to add stiffness. The shear reinforcement was modeled by a two-node numerically integrated truss element because the effect of bending was negligible. The bond-slip between the concrete and reinforcement was not considered in the analyses because an additional reinforcement was installed to avoid a bond splitting failure. The prescribed prestress was introduced into the shear reinforcement, then an axial load was applied with load control in ten steps up to the designated axial load ratio, and finally the shear load was applied with displacement control and a step of 0.01 mm. The maximum-tensile-stress criterion of Rankine was adopted as the failure criterion in the tension zone of concrete. According to this criterion, a crack arises when the maximum principal stress exceeds the tensile strength, regardless of the normal or shearing stresses that occur on other planes. Smeared cracking and bi-linear tension softening, which are shown in Fig. 2, were adopted in the analyses. The shear stiffness of cracked concrete generally depends on the crack width. This phenomenon is taken into account by decreasing the shear stiffness as the normal crack strain increases.

### *2.4 Mechanical Properties of Confined Concrete*

Drucker-Prager criterion was used as the failure criterion in the compressive zone of concrete. The formulation is given by

$$f(I_1, J_2) = \alpha I_1 + \sqrt{J_2} - k = 0 \tag{2.1}$$

$$\alpha = \frac{2\sin\phi}{\sqrt{3}(3-\sin\phi)} \tag{2.2}$$

$$k = \frac{6\cos\phi}{\sqrt{3}(3-\sin\phi)}c \tag{2.3}$$

$$I_1 = \sigma_1 + \sigma_2 + \sigma_3 \tag{2.4}$$

$$J_2 = \left[(\sigma_1-\sigma_2)^2 + (\sigma_2-\sigma_3)^2 + (\sigma_3-\sigma_1)^2\right]/6 \tag{2.5}$$

where $\phi$ is the internal-friction angle, $c$ is the cohesion, $\sigma_1$, $\sigma_2$, and $\sigma_3$ are the principal stresses (see Chen 1982). The internal-friction angle of confined concrete has often been estimated as 37.5° based on the experimental results performed on concrete cylinders with uniform lateral pressure by Richart (1928). According to Richart, the strength of concrete confined by lateral pressure increases to ($\sigma_B$+4.1$\sigma$), regardless of the intensity of $\sigma$, where $\sigma_B$ is the uniaxial compressive strength of concrete and $\sigma$ is the lateral pressure. Takamori et al. (1996, see Fig. 6) studied the effects of lateral confinement using concrete cylinders with different concrete strengths and hoop spacing. According to their test results, the strength of concrete confined by hoops similar to our specimen increases approximately to ($\sigma_B$+2.0$\sigma$), and the effect of confinement decreases as the strength of the concrete and the spacing of hoops increase. An increasing rate to $\sigma$ of 2.0 is less than half of 4.1, which was proposed by Richart (1928) due to the partial confinement by the hoops. This internal-friction angle was estimated as 20°. From these results, the internal-friction angle is assumed as to be 20° for Fc45 and 15° for Fc90. Consequently, Drucker-Prager criterion is as follows:

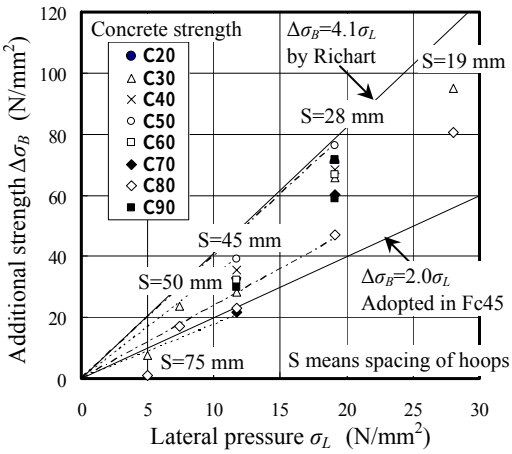


Figure 6 Relationships between lateral pressure and additional strength (Takamori et al. 1996)

$$f(I_1, J_2) = 0.15 I_1 + \sqrt{J_2} - 19.3 = 0 \quad \text{for Fc45} \qquad (2.6)$$

$$f(I_1, J_2) = 0.11 I_1 + \sqrt{J_2} - 42.1 = 0 \quad \text{for Fc90} \qquad (2.7)$$

## 3. SHEAR BEHAVIORS BY EXPERIMENT

### *3.1 Shear Load-Rotation Angle Curves*

Figure 7 shows the shear load $Q$-rotation angle $R$ curves obtained from the tests and compares them to the results of FEM analyses. A typical crack behavior observed during the tests was that flexural cracks initially appeared and then extended into flexural shear cracks near both ends of the specimen. Finally, shear cracks occurred as the shear load increased. The shear loads for both RC and LPRC were gradually reduced without reinforcement yielding because the concrete was crushed in the compressive zone at the top and bottom ends. Table 3 presents the shear crack strength and ultimate shear strength obtained from experiments and FEM analyses as well as the calculation results reported by Watanabe (2004), which consider the lateral prestress. The shear crack strength of analysis is defined as the shear load that causes the strain in the shear reinforcement to increase rapidly. The maximum shear load for the LPRC90-0.15 column was assumed to be 1048 kN when $R$ = -1/50 because the welding of a longitudinal rebar was ruptured in loading to $R$=1/33. When the ratio of axial load for Fc45 series decreased from 0.30 to 0.15, the shear crack strength was reduced by 33% for the RC column and 22% for the LPRC column, and the ultimate shear strength was reduced by 4% for the RC column and 14% for the LPRC column, whereas the rotation angles at the peak load for both columns redoubled. In the Fc45 series, the crack width of RC series rapidly increased immediately after cracking, but the crack width of LPRC series was definitely controlled. The transverse prestressing reduced the width values of shear cracks and increased the shear stiffness after shear cracking. Consequently, this prestressing improved earthquake resistance as well as durability for the RC structures. As shown in Table 3, both FEM analyses and the calculations predict with a fair degree of precision the difference between the shear strength of the RC and LPRC columns. The relationship between shear crack stress, ${}_{exp}\tau_{sc}$ (=${}_{exp}Q_{sc}/bD$), and lateral prestress, and that between ultimate shear stress, ${}_{exp}\tau_{su}$ (=${}_{exp}Q_{su}/bD$), and lateral prestress are plotted in Fig. 8, where the axis of abscissas indicates the ratio of lateral prestress, $\sigma_L$, to compressive strength, $\sigma_B$. The shear crack strength and the maximum shear strength increased with the same rate when the same ratio of $\sigma_L/\sigma_B$ was introduced. Due to an increase in shear crack strength with increasing axial load, the effect of lateral prestress on the shear crack strength decreased as the axial load increased. On the other hand, for the maximum shear strength, the effect of lateral prestress was weakened as the ratio of the axial load to axial strength decreased, which is probably due to the triaxial state of stress in the core concrete and is investigated by FEM analyses in the next section.

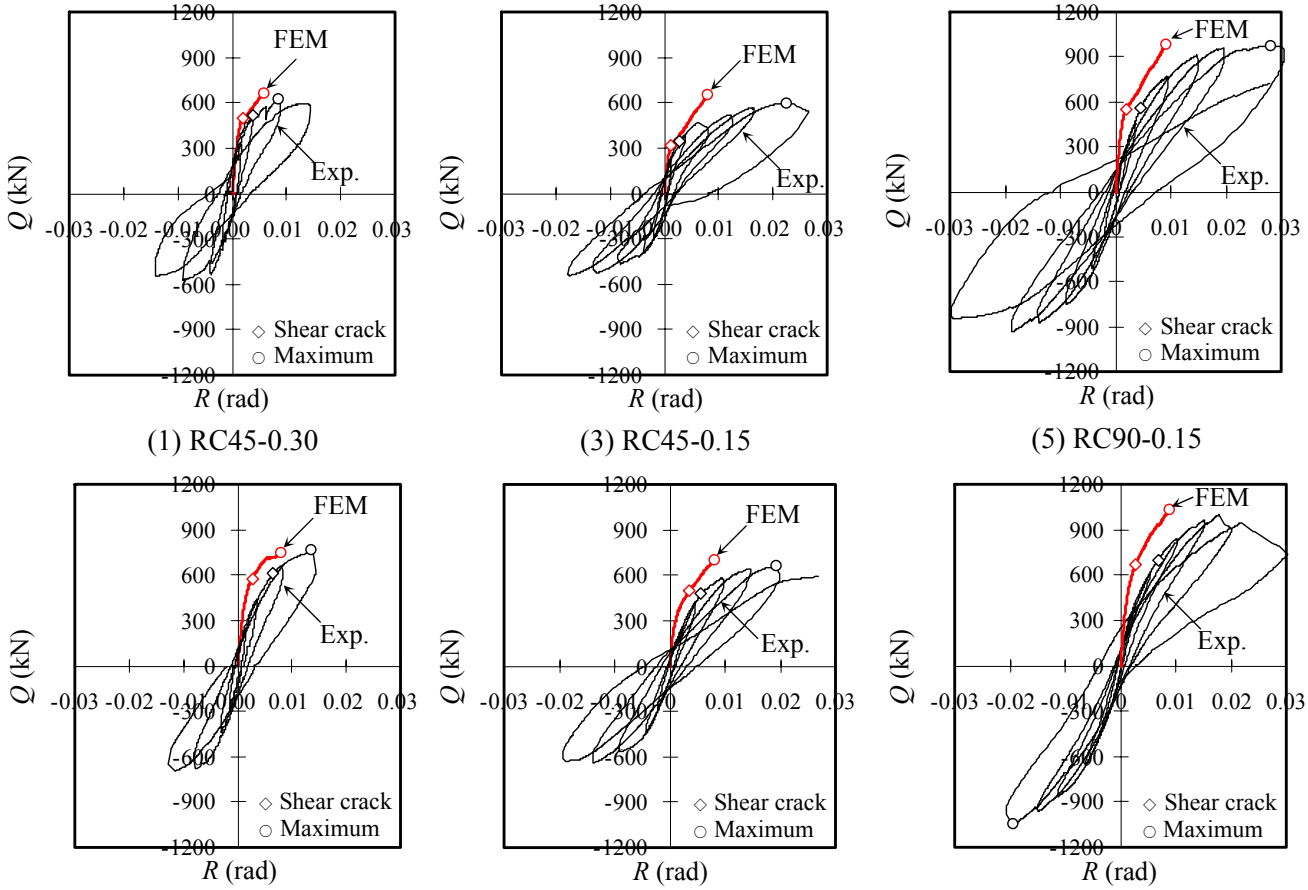


Figure 7 Comparisons between analytical and experimental Q-R curves

Table 3 Shear crack strength and ultimate shear strength

| Test Designation | ${}_{exp}Q_{sc}$ (kN) | ${}_{exp}Q_{su}$ (kN) | ${}_{FEM}Q_{sc}$ (kN) | ${}_{FEM}Q_{su}$ (kN) | ${}_{cal}Q_{sc}$ (kN) | ${}_{cal}Q_{su}$ (kN) |
|---|---|---|---|---|---|---|
| RC45-0.15 | 343 | 595 | 316 | 646 | 339 | 484 |
| LPRC45-0.15 | 475 | 658 | 498 | 699 | 450 | — |
| RC90-0.15 | 562 | 973 | 551 | 983 | 564 | 820 |
| LPRC90-0.15 | 780 | 1048 | 669 | 1027 | 774 | — |
| RC45-0.30 | 515 | 617 | 495 | 655 | 496 | 591 |
| LPRC45-0.30 | 611 | 762 | 577 | 747 | 606 | — |

${}_{exp}Q_{sc}$ =shear crack strength by experiment, ${}_{exp}Q_{su}$ =ultimate shear strength by experiment, ${}_{FEM}Q_{sc}$ =shear crack strength by FEM, ${}_{FEM}Q_{su}$ =ultimate shear strength by FEM, ${}_{cal}Q_{sc}$ =shear crack strength by ref.(1), ${}_{cal}Q_{su}$ =ultimate shear strength by modified Arakawa

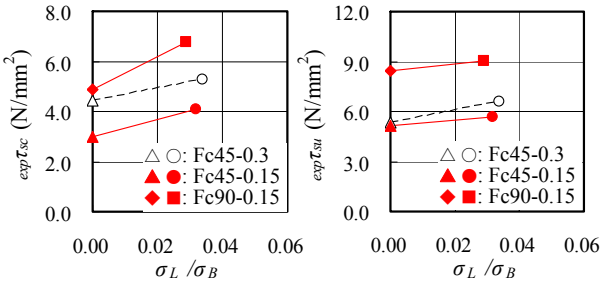


(1) Shear crack strength (2) Ultimate strength

Figure 8 Increase in shear strength due to lateral prestress

### *3.2 Shear Crack Patterns*

Figure 9 compares the shear cracks in the front of RC and LPRC specimens at maximum shear loads. Moreover, the figure shows the location with the maximum crack width and the inclination of the primary shear crack. The crack patterns in the front and back of the specimens were similar. The lateral confinement in the LPRC specimen greatly restrained the shear cracks from propagating so that the final crack pattern of the LPRC drastically differs from that of the RC. Shear cracks developed extensively in the upper and lower sides of the LPRC specimen, but they developed intensively in the center of the RC specimen. The spacing and width of the scattered cracks in the LPRC specimen were smaller than those of the localized cracks in the RC specimen.

Because the ability to transmit shear force across a rough crack is exponentially reduced as crack width increases (Shinohara et al. 1999), a scattered crack with a smaller width can, to some extent, reduce the decrease in shear stiffness of a column. This small crack spacing in the LPRC specimen is probably due to an increase in both bond strength and tensile stress, which were generated by introducing lateral prestress.

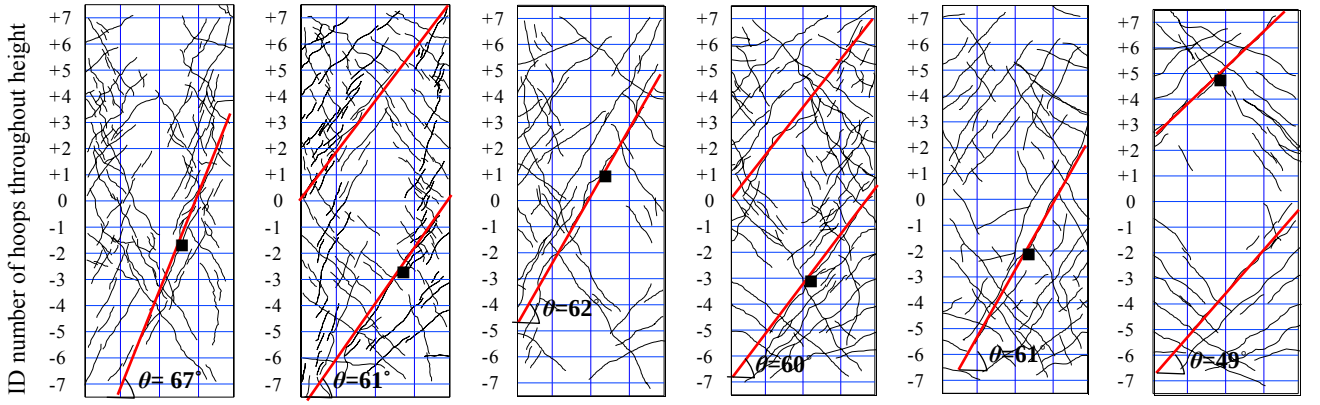


Figure 9 Crack patterns at maximum shear loads

## 4. TRIAXIAL STATE OF STRESS BY ANALYSES

The effect of the lateral confinement on the shear behavior was evaluated based on the triaxial state of stress in the concrete from 3D finite element analyses performed on the RC and LPRC specimens. Figure 10 shows the distributions of the minor principal stress in the center of the RC and LPRC specimens at the maximum loads. The analyses were also performed on the Fc90-0.15 specimens with a diameter of 6.4 mm for shear reinforcement (U6.4) in order to exclude the effect of its quantity. For the specimens with an axial load ratio of 0.3, introducing lateral prestress broadened the width of the compressive strut formed by a large compressive stress at the maximum load. Consequently, the ultimate shear strength became higher than the RC specimen. This difference is probably due to the crack patterns of the RC and LPRC specimens described above. On the other hand for the LPRC45-0.15 specimen, the width of the strut did not increase much because the smaller axial load lessened the confining effect from the triaxial state of compressive stress. For the specimens with a diameter of 9.0 mm for the shear reinforcement (U9.0), a relatively broad strut was formed due to the distributed crack pattern, and a substantial increase in the width of the strut did not occur in the LPRC specimen. For the LPRC90-0.15 specimen with U6.4, the strut width and the maximum shear load were approximately the same as the RC specimen because the shear reinforcement yielded around the peak load.

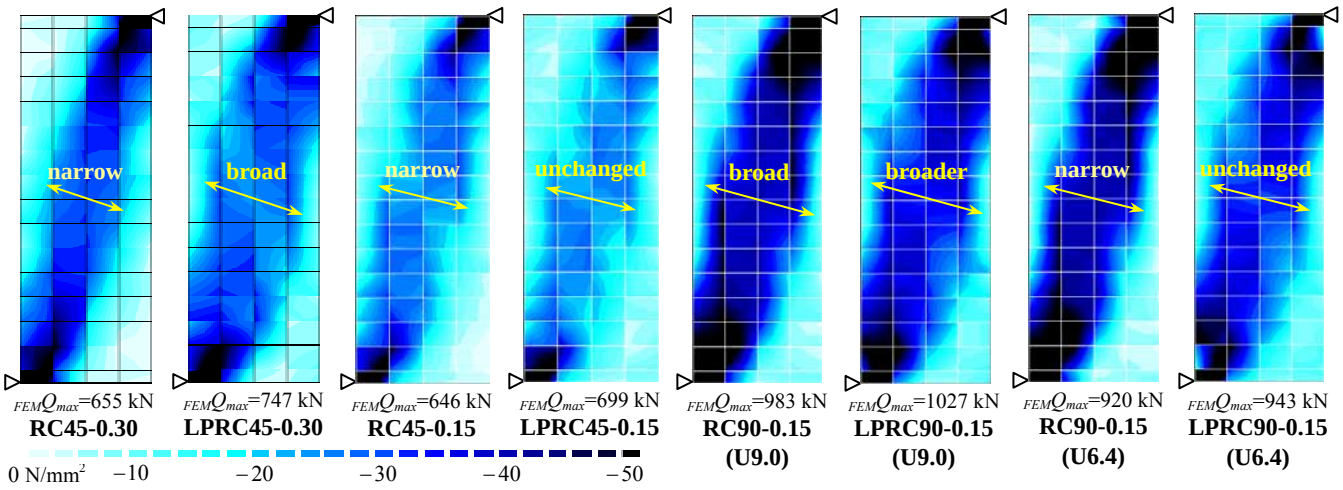


Figure 10 Compression strut based on minor principal stress at maximum shear loads

The degree of damage for compressive failures and the equivalent confining pressure were introduced as gauges to quantitatively evaluate the effect of active confinement on the stress state in the core concrete, as shown in Fig. 11. The degree of damage for compressive failures was defined using the deviated part of the stress state in principal stress space. Figure 12 shows the degree of damage for compressive failures in the surface of the RC and LPRC specimens at the maximum shear loads. Figures 10 and 12 show that the distributions of the degree of damage correspond roughly to those of the minor principal stress. The degree of damage in the LPRC specimen compares favorably with that in the RC specimen at the same shear load due to active confinement (Shinohara et al. 2005). The red parts dotted with a white dot at the top and bottom ends (Fig. 12) represent the post-peak softening zone of concrete. Thus, the failure mode of analyses is quite similar to that of experiment. In a similar way to the width of the compressive strut, introducing lateral prestress enlarged post-peak softening zone, but the effect of the lateral prestress was weakened as the axial load decreased. Compared to the Fc45 specimen, the softening zone in the Fc90 specimen is limited to a small area in the corner, and the effect of the lateral prestress is lessened despite the diameter of shear reinforcement. Furthermore, the degree of damage in the Fc90 specimen is, on the whole, less than that in the Fc45 specimen. This indicates that the collapse of high-strength concrete is chiefly caused by a localized fracture process zone even if most portions are not damaged much, and that high-strength concrete is sensitive to the scale effect. Therefore, it is important for high-strength concrete to have a number of shear reinforcements and to improve resistance to the localized fracture by a substantial confinement.

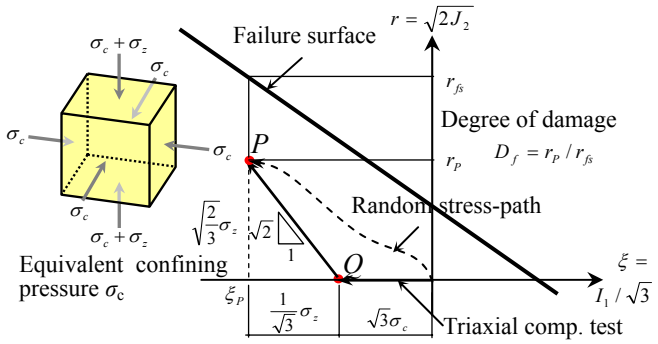


Figure 11 Degree of damage and equivalent confining pressure for triaxial state of stress in meridian plane of Drucker-Prager criterion

The equivalent confining pressure is defined as the lateral pressure when the stress state on a random stress-path is converted into that on the stress-path according to the triaxial compressive test with a constant lateral pressure, as shown in Fig. 11. Consequently, the equivalent confining pressure increased as the hydraulic component increased and as the deviated component of the stress state decreased in the principal stress space. Figure 13 shows an inside view of the ratio of the equivalent confining pressure to the strength of concrete in order to compare RC with LPRC at maximum shear loads. As for the RC45-0.30 specimen, although a very small passive confinement was induced in the RC specimen by applying the axial load, it vanished with an increase in the shear load by 400 kN (Shinohara et al. 2005). Moreover, as shown by Figs. 10 and 13, further increasing the shear load caused the equivalent confining pressure to increase in the same area where the compressive stress grew larger and became localized. For the LPRC45-0.30 specimen, an active confinement, which is over ten times higher than the passive confinement, was produced after applying an axial load (Shinohara et al. 2005). The active confinement covered wider parts of the specimen than the RC specimen until the maximum shear

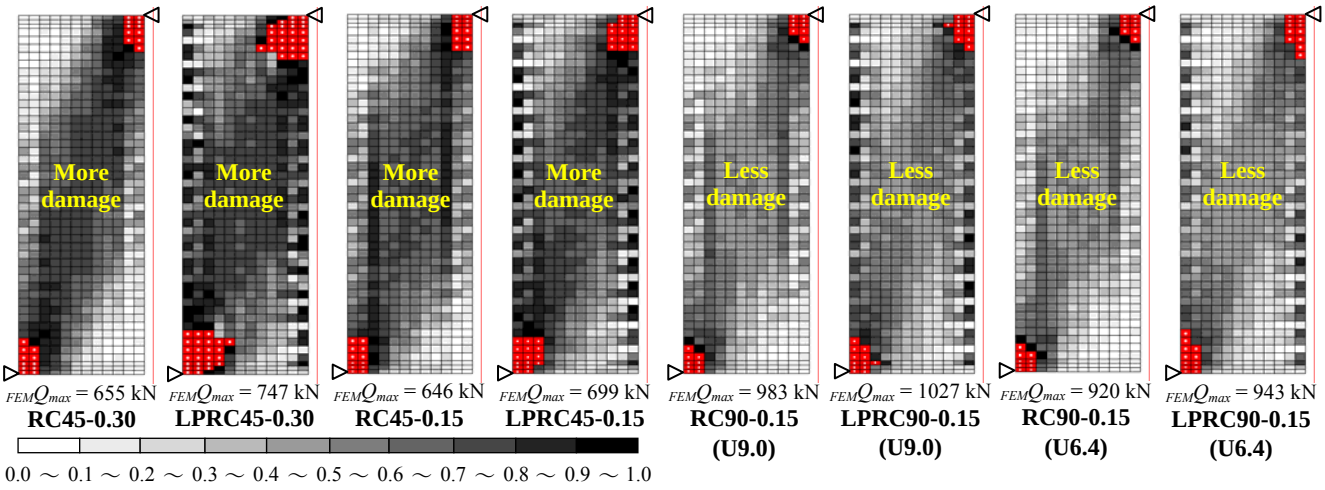


Figure 12 Comparison of the degree of damage for compressive failures

load was reached. Decreasing the axial load ratio from 0.30 to 0.15 locally increased the equivalent confining pressure of the RC specimen, but did not increase the shear resistance. On the other hand, the equivalent confining pressure of the LPRC45-0.15 specimen is obviously lower than that of the LPRC45-0.30 specimen in order for the effect of the lateral prestress to be weakened. The Fc90-U9.0 series shows a relatively high confining pressure because the large quantity of shear reinforcement is arranged regardless if lateral prestress is introduced. Although the zone of high confining pressure of the RC90-U6.4 specimen, which has a smaller shear reinforcement, is localized diagonally compared to the RC90-U9.0 specimen, the zone is extended like the LPRC90-U9.0 specimen upon introducing lateral prestress.

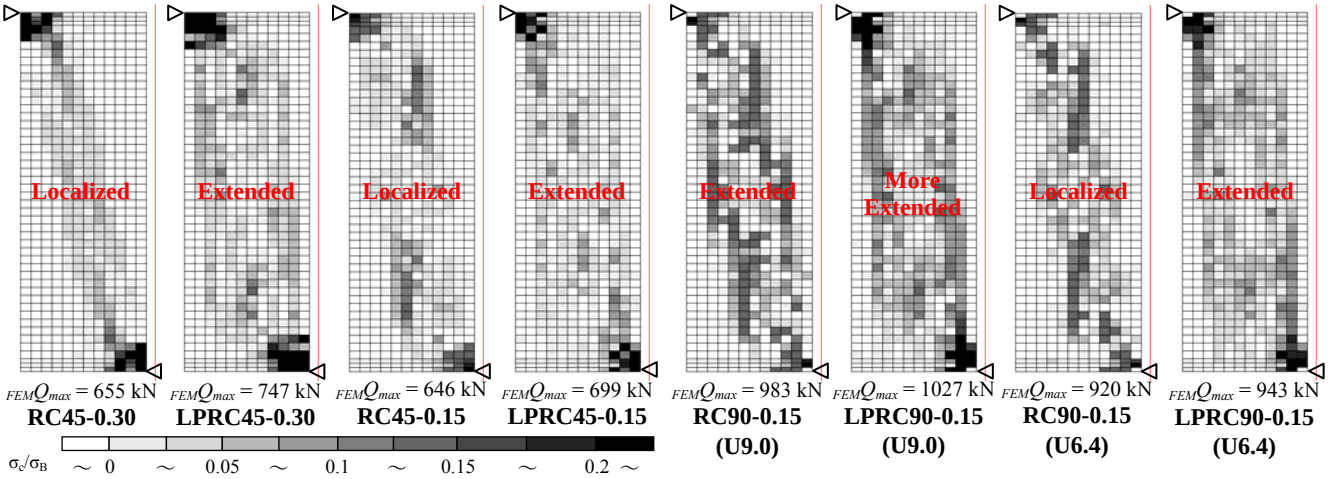


Figure 13 Comparisons of equivalent confining pressure at maximum shear loads

## 5. CONCLUSIONS

1) The shear crack strength and maximum shear strength increase at the same rate upon introducing the same ratio of lateral prestress to compressive strength.
2) Although the ultimate shear strength increases with lateral prestress, the effect of active confinement by the lateral prestress is weakened as the axial load decreases.
3) The effect of the lateral prestress is concealed as the shear reinforcement increases because a distributed crack pattern similar to a LPRC specimen is formed.
4) High-strength concrete is sensitive to the scale effect because the collapse of high-strength concrete is mainly caused by a localized fracture process zone even if most portions are not damaged much.
5) Although the shear stiffness after shear cracking declines for specimen with smaller shear reinforcement, introducing lateral prestress improves considerably.

## REFERENCES

Watanabe, H. et al. (2004). Shear crack control by lateral prestress on reinforced concrete column and evaluation of shear strength. *J. Struct. Const. Eng.*, AIJ, **No.577**, pp.109-116 (in Japanese)
Architectural Institute of Japan (1999). Design Guidelines for Earthquake Resistant Reinforced Concrete Buildings Based on Inelastic Displacement Concept. (in Japanese)
Shinohara, Y. et al. (2005). Active confining effect and shear crack behavior for R/C columns prestressed laterally. *J. Struct. Const. Eng.*, AIJ, **No.587**, pp.147-153 (in Japanese)
Chen, W. F. (1982). Plasticity in Reinforced Concrete. McGraw-Hill Book Company
Richart, F.E., Brandtzaeg, A. and Brown, R. L. (1928). A Study of the Failure of Concrete under Combined Compressive Stresses, *Univ. of Illinois*, *Engineering Experiment Station, Bulletin*, **No.185**
Takamori, N. et al. (1996). Idealization of Stress-Strain Relationship of Confined Concrete, *Proceedings of the Japan Concrete Institute*, **Vol.18**, **No.2,** pp.395-400 (in Japanese)
Shinohara, Y. and Kaneko, M. (1999). Compressive shear behavior in fracture process zone of concrete. *Journal of Structural and Construction Engineering*, AIJ, **No.525**, pp.1-6 (in Japanese)